AIP | Journal of Applied Physics

Epitaxial growth of Bi2Se3 topological insulator thin films on Si (111)

Liang He, Faxian Xiu, Yong Wang, Alexei V. Fedorov, Guan Huang et al.

Citation: J. Appl. Phys. **109**, 103702 (2011); doi: 10.1063/1.3585673
View online: http://dx.doi.org/10.1063/1.3585673
View Table of Contents: http://jap.aip.org/resource/1/JAPIAU/v109/i10
Published by the American Institute of Physics.

Epitaxial growth of Bi_2Se_3 topological insulator thin films on Si (111)

Liang He,[1,a)] Faxian Xiu,[1] Yong Wang,[1,2] Alexei V. Fedorov,[3] Guan Huang,[1] Xufeng Kou,[1] Murong Lang,[1] Ward P. Beyermann,[4] Jin Zou,[2] and Kang L. Wang[1]
[1]*Department of Electrical Engineering, University of California, Los Angeles, California 90095, USA*
[2]*Materials Engineering and Centre for Microcopy and Microanalysis, University of Queensland, Brisbane QLD 4072, Australia*
[3]*Advanced Light Source Division, Lawrence Berkeley National Laboratory, 1 Cyclotron Road, Berkeley, CA 94720, USA*
[4]*Department of Physics, University of California, Riverside, California 92521, USA*

(Received 1 February 2011; accepted 1 April 2011; published online 17 May 2011)

In this paper, we report the epitaxial growth of Bi_2Se_3 thin films on Si (111) substrate, using molecular beam epitaxy (MBE). We show that the as-grown samples have good crystalline quality, and their surfaces exhibit terracelike quintuple layers. Angel-resolved photoemission experiments demonstrate single-Dirac-conelike surface states. These results combined with the temperature- and thickness-dependent magneto-transport measurements, suggest the presence of a shallow impurity band. Below a critical temperature of ~100K, the surface states of a 7 nm thick film contribute up to 50% of the total conduction. © *2011 American Institute of Physics*. [doi:10.1063/1.3585673]

I. INTRODUCTION

Since the prediction of the existence of 3D topological insulators (TIs) in group *V-VI*[1–4] in 2007, this research field has been developing rapidly from theoretical to experimental studies. The 3D TIs have a semiconductor gap in the bulk and a gapless surface state, providing a spin-quantum-Hall-like behavior with quantized conductance of charge and spin in the absence of magnetic field.[4–6] Due to its strong spin-orbit interaction, the direction of spin and moment of the surface electrons is locked; thus the surface conduction electrons are protected by time-reversal-symmetry.[6]

Among all potential 3D TIs, Bi_2Se_3 has a large bulk bandgap of around 0.3 eV, providing great potential for room-temperature applications. Despite a long history of Bi_2Se_3 as a traditional thermoelectric material,[7] not until very recently have the topological surface states been observed by angle-resolved photoemission spectroscopy (ARPES).[8] However, direct evidence of surface states in transport measurements is challenging because of interference from a dominant bulk contribution in TI materials. Usually Bi_2Se_3 is heavily *n*-type doped arising from the Se vacancies.[9–11] The unintentional doping prohibits the surface states from being detected during transport measurements, thus limiting the practical applications.

To overcome the high electron-doping problem, post-growth annealing in a Se-rich environment[11] and Ca counter-doping[12,13] have been studied. With traditional stoichiometric melts of Bi and Se in a crucible, systematic doping control is very difficult and influenced by local compositional fluctuations. On the other hand, the thin film growth by molecular beam epitaxy (MBE) has tremendous advantages, such as excellent doping control, a reduction of the bulk contribution, the possibility of surface engineering, and potential integration of heterostructures and/or superlattices for more complex device structures. To date, there have been very few reported studies using this growth technique[14–16] and, to the best of our knowledge, the transport properties of TI thin films grown with MBE have not been investigated. In this study, we report the epitaxial growth of Bi_2Se_3 thin films using a solid source MBE. We show that the as-grown samples have good crystalline quality, and their surfaces exhibit terracelike quintuple layers. Most importantly, our ARPES experiments unambiguously demonstrate single-Dirac-conelike surface states. These results are qualitatively in agreement with our temperature- and thickness-dependent magneto-transport measurements, suggesting the presence of a shallow impurity band. By systematically studying the magneto-transport, we conclude that the surface states, contributing up to 50% of the total conduction, dominate the conduction below a critical temperatures of ~100K, for the thin film with a thickness of 7 nm, comparable to our recent findings in gated Bi_2Te_3 nano wires.[17]

II. EXPERIMENTS

The thin film growth was carried out with a Perkin Elmer MBE system. The Si (111) substrates were first cleaned by a standard RCA procedure before being loaded into the growth chamber. The Si substrates were then annealed at 550 °C to eliminate hydrogens bonding on the surface. High-purity Bi (99.9999%) and Se (99.99%) sources were evaporated by conventional effusion cells. During the growth, Bi and Se effusion cells were kept at 490 and 200 °C respectively, while Si (111) substrate was set at 150 °C. The surface of the Bi_2Se_3 was monitored by the RHEED technique and found to be atomic flat as evidenced by streaky RHEED patterns. The digital images of RHEED were captured using a KSA400 system made by K-space Associates, Inc.

[a)]Author to whom correspondence should be addressed. Electronic mail: heliang@ee.ucla.edu.

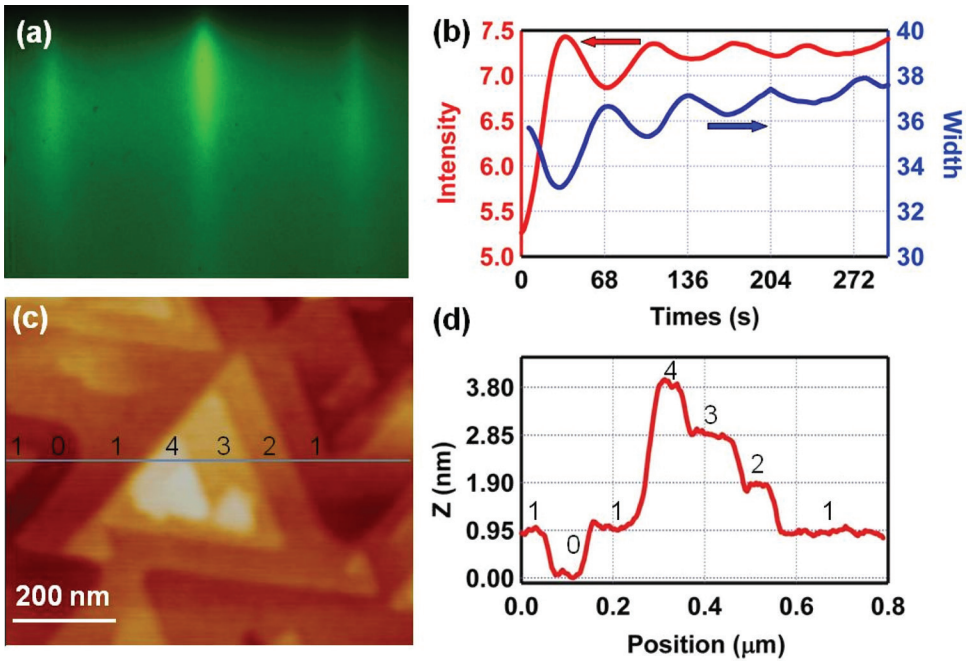

FIG. 1. (Color online) (a) RHEED patterns of an as-grown surface of Bi_2Se_3 with a thickness of 44 nm. (b) RHEED oscillations of the intensity (upper red) and width (lower blue) of the specular beam. The oscillation period is found to be 68 s, corresponding to a growth rate of ~0.9 QL/min. (c) Large area AFM image of Bi_2Se_3 film (size: 0.8 μm × 0.7 μm). (d) The height profile along the gray line marked in Fig. 1(c) showing a step size of 0.95 nm.

The high-resolution TEM experiments were performed on a FEI Tecnai F20 (S)TEM operating at 200 KV. The digital images were recorded by a Gatan® 2k × 2k CCD camera.

High-resolution ARPES experiments were performed at beam line 12.0.1 of the Advanced Light Source at LBNL, using 100 eV and 52 eV photons for measuring core levels and surface states, respectively. For the low temperature transport measurements, a standard Hall bar geometry with a channel size of ~3 mm × 0.3 mm was fabricated through a conventional photolithograph method. A physical property measurement system (PPMS) manufactured by Quantum Design was used to measure the magneto-transport properties.

III. RESULTS AND DISCUSSION

The Bi_2Se_3 thin films were grown in an ultrahigh vacuum MBE system. Real-time reflection high energy electron diffraction (RHEED) was used to monitor the *in situ* growth dynamics with the electron beam incidences along the $[11\bar{2}0]$ direction. Figure 1(a) shows the RHEED pattern of a Bi_2Se_3 film with a thickness of 44 nm. The sharp streaky lines indicate a flat surface morphology; thus the growth is smoothly pseudomorphic. Figure 1(b) shows the time dependent evolution of the intensity (upper red curve) and transverse width (lower blue curve) of the specular spot during the growth. Layer-by-layer RHEED oscillations can be clearly observed with a period of ~68 s, or 0.9 QL/min. The 180° phase shift between the intensity and width provides strong evidence that the oscillations come from the periodical change of the surface morphology,[18] excluding artifacts such as system vibrations during the growth. At the early stage of the growth, we also observed the diffraction patterns reflecting 3D growth mode in addition to the 2D streaky lines and the specula spot. These 3D spots diminish quickly as the growth continues and completely disappear after 8 QLs. The 3D transmission pattern is probably caused by the formation of small islands, and as the film becomes thicker, islands merge together to produce a flat plateau.

Figure 1(c) shows a large-scale atomic force microscope (AFM) image of an as-grown Bi_2Se_3 film with a thickness of 44 nm, exhibiting individual terraces. The surface consists of characteristically triangle-shaped terraces and steps, reflecting the hexagonal crystal structure inside of the (0001) plane.[19] Figure 1(d) displays a height profile of the gray line marked in Fig. 1(c). The height of each step is ~0.95 nm, consistent with a single QL thickness.

In addition to the AFM study, high-resolution transmission electron microscopy (HRTEM) was performed to investigate the film quality. Figure 2(a) shows a HRTEM image taking along the Si [110] direction. As can be seen, on top of the Si (111) substrate, an amorphous interface layer of ~1.7 nm and a Bi_2Se_3 thin film of ~7 nm can be observed. It should be noted that the projected period along the c axis is 0.955 nm, as indicated in Fig. 2(a), fitted well the Bi_2Se_3 crystal structure with the lattice parameters of $a = 0.414$ nm and $c = 2.864$ nm. Figures 2(b) and 2(c) show the energy dispersive spectroscopy (EDS) of this Bi_2Se_3 film and the interface layer. Within the Bi_2Se_3 film, the signatures of Bi and Se can be identified in addition to carbon (C, from the epoxy), copper (Cu, from TEM grid) and a trace of silicon (Si, from the substrate). As a comparison, within the interfacial layer, we can only indentify Se and Si without a hint of Bi. This fact suggests that the amorphous interface layer is probably $SiSe_2$.[20] We anticipate that such an amorphous layer may be formed in the Se rich environment and during the initial 550 °C annealing.

The electronic structure of the films was verified by using ARPES. The measurements have been performed at BL12 of the Advanced Light Source using essentially the same setup which has been employed for the first ARPES

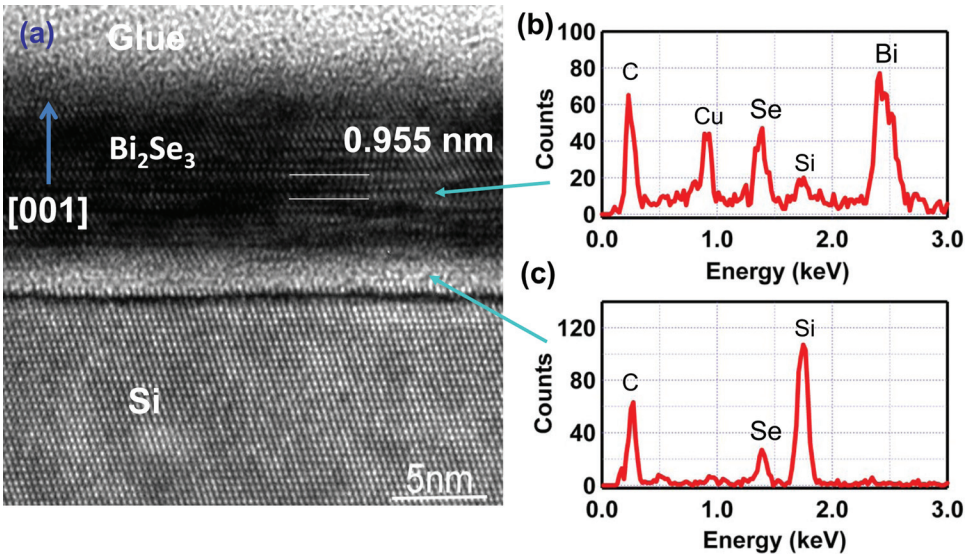

FIG. 2. (Color online) (a) High-resolution transmission electron microscopy (HRTEM) of a 7 nm Bi_2Se_3 grown on a Si (111) substrate. The lattice space of (003) plane is 0.955 nm. (b) and (c) the energy dispersive spectroscopy (EDS) of the film and interface, respectively.

studies of bulk crystals of TIs.[21] Contrary to the bulk crystals, however, atomically clean surfaces of our samples could not be prepared by cleaving them in vacuum. Hence, in the present study, prior to the measurements samples were annealed at 200 °C for 2 to 3 h. Vacuum during annealing stayed below 6×10^{-10} Torr. Core-level spectroscopy and ARPES were performed with 100 eV and 52 eV photons, respectively, with the samples held at room temperature. Figure 3(a) displays 3*d* and 5*d* core levels (spin-orbit split doublets) of Se and Bi, respectively. The fact that no extra peaks were observed indicates a good surface quality with a *stoichiometric* composition. An important confirmation comes from the ARPES data plotted in Fig. 3(b). The data reveal a familiar surface state with a linear dispersion crossing the Fermi level. This state is the key TI characteristics, which has been extensively studied on the surfaces of bulk crystals.[8,13,21]

The transport measurements of TI thin films are a critical gauge for determining material properties and a prestep needed to realize TI based devices. As plotted in Fig. 4(a), the temperature-dependent resistivity of four samples with different film thicknesses exhibits the same characteristic behavior. The resistivity first decreases monotonically as the temperature decreases from room temperature; the metallic resistivity indicates phonon scattering dominantes the temperature dependence over this range. After reaching a minimum between 70 and 170 K, depending on the thickness of samples, the resistivity exhibits an exponential increase with respect to 1/T. In the low temperature region, however, the resistivity of all the samples saturates at a constant value. This temperature-dependent behavior is consistent with the "*nonmetallic crystals*"[22] where the Fermi energy sits within the gap between the bulk conduction band and valence band.

In the high temperature region above 130 K, the resistivity of the three thickest films collapses onto one curve, invariant of the film thickness. This indicates that at those temperatures the resistivity is dominated by the bulk conductance. Figure 4(b) exhibits the conductivity after substrated the plateau value-the surface states dominated conductation, as a function of 1/T. For the films with thicknesses above 10 nm, the bulk properties are fully developed with a common activation energy of ~37 meV, as shown by the right three dotted lines in Fig. 4(b). This is most likely associated with a shallow impurity band[23] from Se vacancies with a level of about 37 meV lower than the bulk conduction band. However, the thinnest film with a thickness of 7 nm behaves slightly different. In the high-temperature region where bulk conductance dominates, the resistivity is slightly lower than the thicker samples,

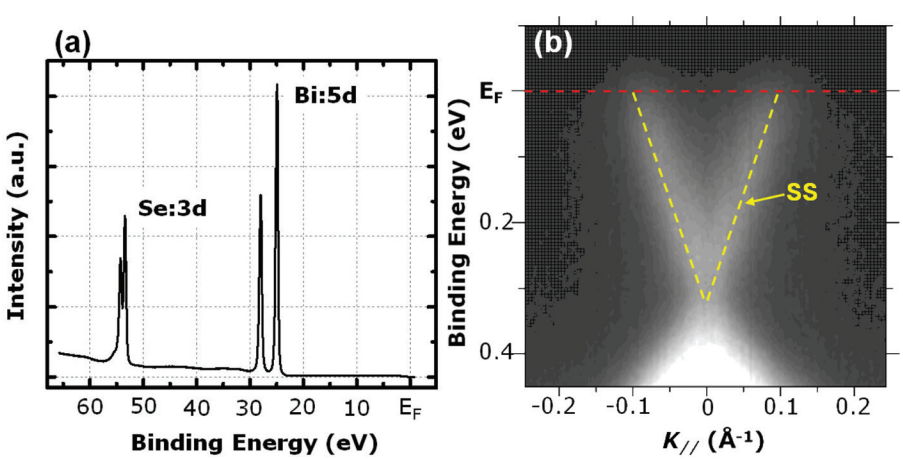

FIG. 3. (Color online) (a) Core level photoemission and (b) Angle Resolved Photoemission data taken from sample consisting of 44 nm of Bi_2Se_3 grown on Si(111). (a) Core levels of Se and Bi measured with 100 eV photons. (b) The V-shaped surface state crossing the Fermi level. APRES data were taken using 52 eV photons.

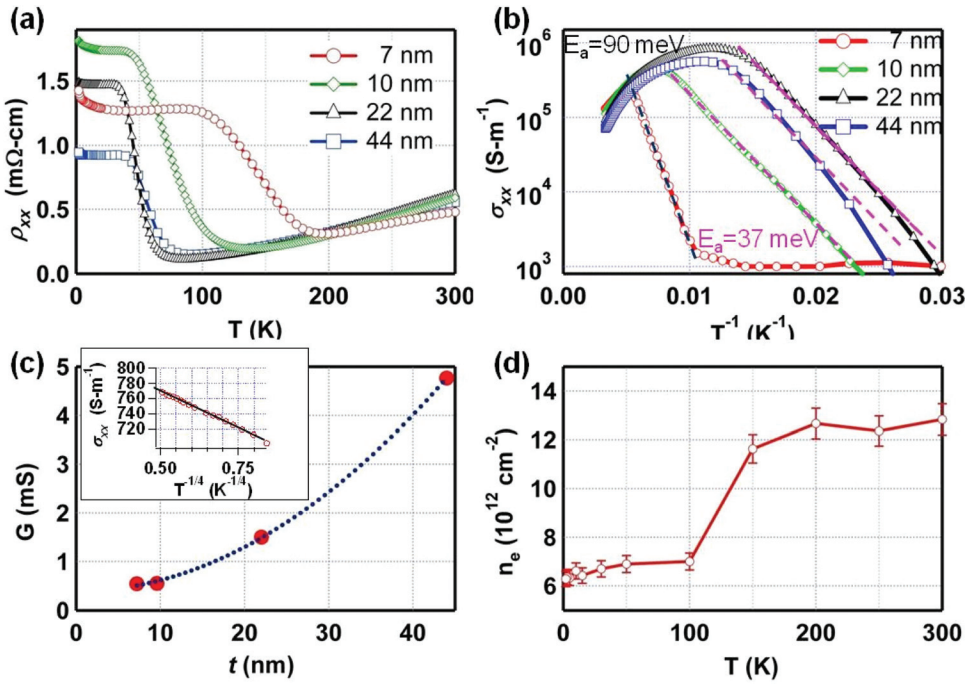

FIG. 4. (Color online) (a) Resistivity of four samples with different thicknesses versus temperature. (b) Conductivity vs $1/T$. The left (black) dashed line indicates a low temperature activation energy of about 90 meV. The right three (purple) dashed lines indicate an activation of about 37 meV. (c) Conductance versus thickness at $T = 20$K. The blue dotted line is a parabolic fit. The inset shows σ_{xx} versus $T^{-1/4}$ for the 7 nm think film. Please note that the vertical axis is plotted in log scale. The linear line represents $\log(\sigma_{xx}) \propto T^{-1/4}$. (d) Sheet carrier density of a 7 nm thick film as a function of temperature.

suggesting that the total conductance has a bigger contribution from the surface states. Also, the activation energy of 90 meV (the left dotted line in Fig. 4(b)), indicates a deeper donor level, probably bearing less impurity states. We also noticed that over time the ambience environment has subtle influence on ultrathin films (in terms of impurity activation energy), while much less effect on the thicker films.

As the temperature drops below the activation region where the bulk carriers freeze out, the transport is presumably dominated by carriers in the surface states and impurity band hopping. In this region, the sheet conductance is almost temperature independent with a value that monotonically decreases with decreasing the film thickness, as shown in Fig. 4(c). This variation of the conductivity in the saturation regime with the film thickness mostly comes from the bulk effect such as impurity band hoping. The thicker the film, the more the states in the impurity band, and hence the more the conduction. By fitting the conduction with a parabolic curve line (blue dashed line in Fig. 4(c)), it is possible to extrapolate the conductivity toward zero thickness and provide a good estimation of the surface state conduction, $\sim 3.9 \times 10^{-4}$ S.

Below 10K, the resistivities of all samples exhibit another small increase. The conductance follows a typical Mott $T^{-1/4}$ law down to 2K, (as shown in the inset of Fig. 4(c)), indicating that the variable range hopping is the dominant mechanism for transport in the impurity band.[24,25]

Hall measurements were also preformed on these films. An example is shown in Fig. 4(d), in which the sheet carrier density is plotted as a function of the temperature for the thin film with the thickness of 7 nm. When the temperature is higher than 200K, the measured sheet carrier density saturates at approximately 1.25×10^{13} cm^{-2}, reflecting contributions from surface carrier and bulk conduction band electrons excited from an impurity band. As the temperature drops below 200K, the sheet carrier density quickly decreases to $\sim 7 \times 10^{12}$ cm^{-2} and then a further small dips occurs at even lower temperatures. This temperature-dependence of the sheet carrier density is consistent with our previous conclusion from resistivity data. In other words, there is an impurity band below the bulk conduction band, and thermally excited electrons in the bulk conduction band are frozen out when the temperature drops below ~100K. Based on this analysis, we can estimate the surface density n_s to be 7×10^{12} cm^{-2}, and the bulk carrier density n_b to be 7×10^{18} cm^{-3}, consistent with other reports.[11] It is interesting to note that the carrier density of the surface states accounts for up to 58% of the total carriers in this thin film.

At $T = 5$K, the longitudinal magneto-resistance (MR) with the field parallel to the current and perpendicular to the c-axis is plotted in Fig. 5(a) for films with different thicknesses, in which the MR is defined as $\mathrm{MR} = \rho_{xx}(\mathrm{B})/\rho_{xx}(0)$-1. The two thicker films have a sharp cusp at low magnetic field, which is a clear signature of weak anti-localization (WAL) effect originating from the spin-orbit interaction.[22,26,27] Contrary to this behavior, the 7 nm thick film show a semiclassical parabolic field dependence at low fields, and the MR of the intermediate thick film (10 nm) sits between these two extremes. Since the magnetic field is in-plane, 2D WAL should not be observed. Therefore, we conclude the phenomenon is 3D WAL at low temperature and originates from the impurity band electrons in the bulk.

It is also interesting to note that, at high magnetic fields, the MR for other thicker films has a clearly linear dependence on the field, as shown in Fig. 5(b). This has been identified as the quantum linear Hall effect,[28,29] where the large linearity is predominantly caused by coupling of the spin to the field. The thinner films also have a trace of linearity at

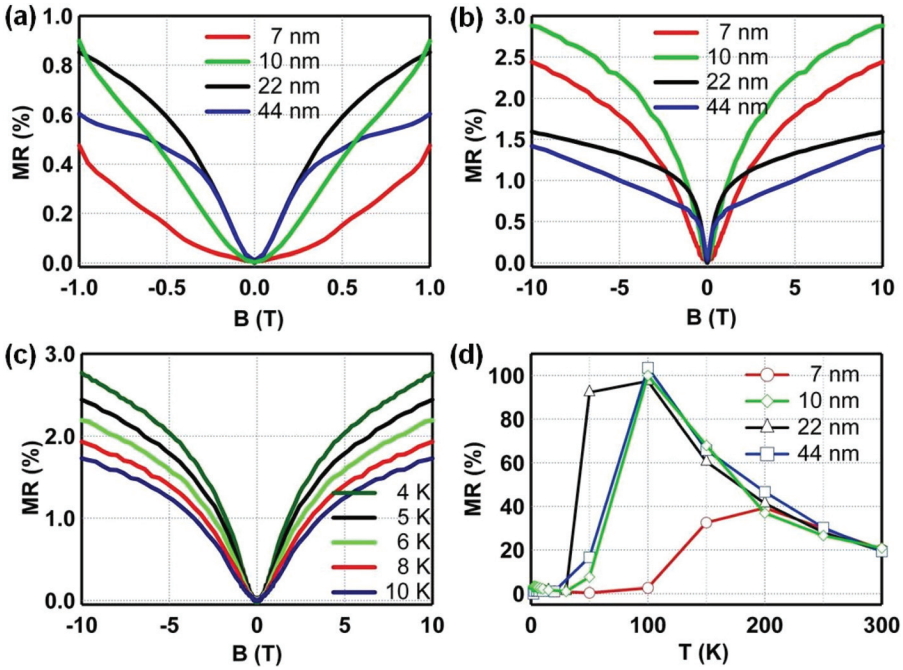

FIG. 5. (Color online) Magneto-resistance Bi_2Se_3 thin films for four different thickness at 5 K with low (a) and high magnetic fields (b). (c) MR of a 7 nm film at temperatures from 4 to 10 K. (d) MR with respect to temperature when $B = 10$ T.

very high field. Figure 5(c) shows the MR of the 7 nm thick film at several temperatures between 4K and 10K, where universal conductance fluctuation (UCF)[30] can be observed at low temperature and high magnetic field.

Finally, the temperature-dependence of the MR for all the films is shown in Fig. 5(d). At high temperatures (100 ~ 300K) where the bulk conduction dominates, the MR is relatively large (20–100%) and increases as the temperature decreases. The large MR here is presumably due to the enhanced phonon scattering by the magnetic field. As soon as the temperature drops to the points where the electrons are frozen (i.e., 50 to 100K), the MR decreases rapidly to a value of 2%. Since the conduction mechanism for the surface electron and impurity band electron is insensitive to scattering, the magnetic field should have a much weaker effect on the transport. As temperature decreases, the drastic change of MR probably reflects the transition from bulk conductance to surface electron transport and impurity band electron hopping, consistent with Fig. 4.

IV. SUMMARY

In summary, we have epitaxially grown high-quality Bi_2Se_3 thin films with thickness down to 7 nm by using a MBE system. The ARPES results provide unambiguous evidences of single-Dirac-conelike surface states. Below a critical temperature that depends on the film thickness, a combination of a shallow impurity band hopping and surface-state electron conduction with a contribution of up to 50% has been evidenced. In our ultra-thin Bi_2Se_3 MBE-grown thin films, the successful demonstration of the dominating surface states in magnetotransport measurements, provides a first but yet important step toward the fabrication of multifunctional heterostructures for innovative nanoelectronics and spintronics.

ACKNOWLEDGMENTS

We acknowledge the Focus Center Research Program-Center on Functional Engineered Nano Architectonics (FENA) and the Australia Research Council for their financial supports of this project. Yong Wang thanks the Queensland International Fellowship. The Advanced Light Source is supported by the Director, Office of Science, Office of Basic Energy Sciences, of the U.S. Department of Energy under Contract No. DE-AC02-05CH11231.

[1] L. Fu, C. L. Kane, and E. J. Mele, Phys. Rev. Lett. **98**, 106803 (2007).
[2] J. E. Moore and L. Balents, Phys. Rev. B **75**, 121306 (2007).
[3] H. Zhang, C.-X. Liu, X.-L. Qi, X. Dai, Z. Fang, and S.-C. Zhang, Nat. Phys. **5**, 438 (2009).
[4] L. Fu and C. L. Kane, Phys. Rev. B **76**, 045302 (2007).
[5] B. A. Bernevig, T. L. Hughes, and S. C. Zhang, Science **314**, 1757 (2006).
[6] X. L. Qi and S. C. Zhang, Phys. Today **63**, 33 (2010).
[7] C. B. Satterthwaite and R. W. Ure, Phys. Rev. **108**, 1164 (1957).
[8] Y. Xia, D. Qian, D. Hsieh, L. Wray, A. Pal, H. Lin, A. Bansil, D. Grauer, Y. S. Hor, R. J. Cava, and M. Z. Hasan, Nat. Phys. **5**, 398 (2009).
[9] J. G. Analytis, J. H. Chu, Y. L. Chen, F. Corredor, R. D. McDonald, Z. X. Shen, and I. R. Fisher, Phys. Rev. B **81**, 205407 (2010).
[10] D. S. Kong, W. H. Dang, J. J. Cha, H. Li, S. Meister, H. L. Peng, Z. F. Liu, and Y. Cui, Nano. Lett. **10**, 2245 (2010).
[11] H. Peng, K. Lai, D. Kong, S. Meister, Y. Chen, X. L. Qi, S. C. Zhang, Z. X. Shen, and Y. Cui, Nat. Mater. **9**, 225 (2009).
[12] Y. S. Hor, A. Richardella, P. Roushan, Y. Xia, J. G. Checkelsky, A. Yazdani, M. Z. Hasan, N. P. Ong, and R. J. Cava, Phys. Rev. B **79**, 195208 (2009).
[13] D. Hsieh, Y. Xia, D. Qian, L. Wray, J. H. Dil, F. Meier, J. Osterwalder, L. Patthey, J. G. Checkelsky, N. P. Ong, A. V. Fedorov, H. Lin, A. Bansil, D. Grauer, Y. S. Hor, R. J. Cava, and M. Z. Hasan, Nature **460**, 1101 (2009).
[14] Y. Y. Li, G. Wang, X. G. Zhu, M. H. Liu, C. Ye, X. Chen, Y. Y. Wang, K. He, L. L. Wang, X. C. Ma, H. J. Zhang, X. Dai, Z. Fang, X. C. Xie, Y. Liu, X. L. Qi, J. F. Jia, S. C. Zhang, and Q. K. Xue, Adv. Mater. **22**, 4002 (2010).
[15] H. D. Li, Z. Y. Wang, X. Kan, X. Guo, H. T. He, Z. Wang, J. N. Wang, T. L. Wong, N. Wang, and M. H. Xie, New J. Phys. **12**, 103038 (2010).

[16]G. Zhang, H. Qin, J. Teng, J. Guo, Q. Guo, X. Dai, Z. Fang, and K. Wu, Appl. Phys. Lett. **95**, 053114 (2009).
[17]F. Xiu, L. He, Y. Wang, L. Cheng, L.-T. Chang, M. Lang, G. Huang, X. Kou, Y. Zhou, X. Jiang, Z. Chen, J. Zou, A. Shailos, and K. L. Wang, Nat. Nano **6**, 216 (2011).
[18]J. M. Van Hove, P. R. Pukite, and P. I. Cohen, Journal of Vacuum Science & Technology B: Microelectronics and Nanometer Structures **3**, 563–567 (1985).
[19]A. Richardella, D. M. Zhang, J. S. Lee, A. Koser, D. W. Rench, A. L. Yeats, B. B. Buckley, D. D. Awschalom, and N. Samarth, Appl. Phys. Lett. **97**, 262104 (2010).
[20]R. D. Bringans and M. A. Olmstead, Phys. Rev. B **39**, 12985 (1989).
[21]D. Hsieh, Y. Xia, D. Qian, L. Wray, F. Meier, J. H. Dil, J. Osterwalder, L. Patthey, A. V. Fedorov, H. Lin, A. Bansil, D. Grauer, Y. S. Hor, R. J. Cava, and M. Z. Hasan, Phys. Rev. Lett. **103**, 146401 (2009).
[22]J. G. Checkelsky, Y. S. Hor, M. H. Liu, D. X. Qu, R. J. Cava, and N. P. Ong, Phys. Rev. Lett. **103**, 246601 (2009).
[23]E. Ohta and M. Sakata, Solid-State Electron. **22**, 677 (1979).
[24]R. Jones and W. Schaich, J. Phys. C **5**, 43 (1972).
[25]N. F. Mott, J. Non-Crystal. Solids **1**, 1 (1968).
[26]J. Chen, H. J. Qin, F. Yang, J. Liu, T. Guan, F. M. Qu, G. H. Zhang, J. R. Shi, X. C. Xie, C. L. Yang, K. H. Wu, Y. Q. Li, and L. Lu, Phys. Rev. Lett. **105**, 176602 (2010).
[27]J. G. Checkelsky, Y. S. Hor, R. J. Cava, and N. P. Ong, arXiv: 1003.3883v1 [cond-mat.mes-hall] (2010).
[28]D. X. Qu, Y. S. Hor, J. Xiong, R. J. Cava, and N. P. Ong, Science **329**, 821 (2010).
[29]M. Lee, T. F. Rosenbaum, M. L. Saboungi, and H. S. Schnyders, Phys. Rev. Lett. **88**, 066602 (2002).
[30]P. A. Lee, A. D. Stone, and H. Fukuyama, Phys. Rev. B **35**, 1039 (1987).